J. Min. Metall. Sect. B-Metall. 61 (3) (2025) 369 - 383

Journal of Mining and Metallurgy,
Section B: Metallurgy

EVOLUTION OF MICROSTRUCTURE UNDER DIFFERENT HOMOGENIZATION CONDITIONS AND ITS EFFECT ON RECRYSTALLIZATION PROCESSES DURING HOT ROLLING OF AA5182 ALLOY

Aleksandar Ćitić [a,b], Tamara Radetić [a], Filip Rajković [c], Dejan Prelević [c], Miljana Popović [a,*]

[a] University of Belgrade, Faculty of Technology and Metallurgy, Belgrade, Serbia
[b] Military Technical Institute, Belgrade, Serbia
[c] University of Belgrade, Faculty of Mining and Geology, Belgrade, Serbia

(Received 17 August 2025; Accepted 20 December 2025)

Abstract

This study investigates microstructure development of AA5182 Al-Mg alloy under various homogenization conditions and how these conditions affect recrystallization processes and texture development during the laboratory hot-rolling. Homogenization treatments were conducted for 16 h at 490 °C and for 4 h, 16 h and 96 h at 550 °C. Scanning electron microscopy (SEM) characterization including energy-dispersive X-ray spectroscopy (EDX) revealed the presence of Al_3(Fe,Mn) and Al_m(Fe,Mn) phases as Fe/Mn-bearing microconstituents in the as-cast state. These transformed into Al_6(Fe,Mn) and α-Al(Fe,Mn)Si during homogenization treatments. The treatments also led to precipitation of Al_6(Mn,Fe) and α-Al(Fe,Mn)Si dispersoid particles. The results of electron backscattered diffraction (EBSD) indicated that a weak deformation texture was present after hot-rolling. The morphology of grains and the degree of restoration were significantly influenced by homogenization conditions. The distribution and density of dispersoids had a strong effect on the mechanisms of recovery and recrystallization.

Keywords: *AA5182 alloy; Homogenization; (Fe,Mn)-bearing microconstituents; Mn-bearing dispersoids; Recrystallization*

1. Introduction

AA5182 is a medium strength, magnesium-rich alloy from the 5xxx series, widely used as a structural material. This alloy is typically supplied in sheet form, either as hot-rolled coils or thin, cold-rolled sheets [1]. Being a non-heat-treatable alloy, AA5182 mainly gains strength through solid solution hardening by magnesium solute and work-hardening. However, the presence of secondary intermetallic phases such as microconstituents and dispersoids, their phase composition, morphology and distribution, significantly influence the alloy's plasticity, formability [2−4] and corrosion resistance [5, 6].

Apart from magnesium, the 5xxx alloys contain alloying elements like manganese and chromium, along with unavoidable impurities such as iron and silicon. Transition metals, particularly iron, have low solubility in solid aluminum, which leads to the formation of various intermetallic compounds during the solidification process. The phase selection is affected by solidification rates and the chemical composition, particularly Fe/Si and Fe/Mn ratios [1, 7−10].The impact of solidification parameters is highlighted by the range of Fe/Mn-bearing compounds seen in the as-cast state of AA5182 alloy. Simensen et al. [11] reported Al_6(Fe,Mn) and Al_3(Fe,Cu,Mn) as main Fe-bearing constituents, however other studies did not detect Al_6(Fe,Mn) phase. C.J. Lee et al. [12] identified Al_m(Fe,Mn) and Al_3(Fe,Mn) as the iron-bearing intermetallic phases in the as-cast state, while Engler et al. [8] observed only Al_3(Fe,Mn). N.Tian et al. [13] reported Al_{19}(Fe,Mn) as the Fe/Mn-bearing constituent phase.

Among the steps of thermo-mechanical processing, homogenization annealing has, by far, the strongest influence on the alloy microstructure and microchemistry. The treatment reduces microsegregation, it may affect microconstituents, and leads to dispersoid precipitation. A number of recent studies on 5xxx alloys were directed toward altering chemical composition and/or development of homogenization procedures, usually involving low-temperature homogenization to enhance dispersoid hardening [14, 15]. While two types of dispersoids,

---

Corresponding author: miljana@tmf.bg.ac.rs

https://doi.org/10.2298/JMMB250817029C

acicular $Al_6(Mn,Fe)$ and rounded α-Al(Mn,Fe)Si, were observed to precipitate in an AA5182 alloy [8], the alloy is relatively lean in dispersoid forming elements, making significant dispersoid hardening unlikely. However, the precipitation of finely dispersed Mn-based particles is a key factor influencing recovery and recrystallization during hot-deformation and subsequent thermo-mechanical processing [14−16].

The aim of this study was to document changes in microconstituents and dispersoids induced by various homogenization treatments, and to assess their impact on restoration processes and texture development during a hot-rolling of industrially cast AA5182 alloy. The evolution of the constituent particles and formation of dispersoids under different homogenization treatments was followed by electrical conductivity/resistivity measurements and characterized by scanning electron microscopy (SEM) including electron dispersive spectroscopy (EDS). The study of grain microstructure and texture was conducted by optical microscopy and electron backscattered diffraction (EBSD) technique.

2. Experimental

The material used in this study was a slice of an industrially direct-chill (DC) cast ingot of commercial AA5182 alloy, supplied by Impol Seval Aluminum Mills. The chemical composition of the alloy was analyzed by an optical emission spectrometer (Belec Compact Port HLC) and the results are shown in Table 1.

For experimental processing, blocks measuring 110×60×25 mm were cut from the as-cast slice. Positions of the cut blocks, which were near the half-width at quarter thickness of the slice, are schematically shown in Figure 1. This position is considered to be representative of the final sheet properties, according to [9]. The laboratory thermo-mechanical processing included homogenization treatment followed by a hot-rolling (HR).

A preliminary evaluation of the effect of homogenization conditions on processes taking place during homogenization was conducted by electrical resistivity measurements. The electrical resistivity is highly sensitive to the presence of point defects in the solid solution, including solute atoms, and, as such, has been used for determination of the extent of precipitation/dissolution reactions during heat treatment [17]. The electrical conductivity/resistivity measurements were performed using the Foerster Sigmatest 2.069 instrument, operating at a frequency of f=120 kHz. Samples for electrical resistivity measurements were homogenized for 16 h at 430 °C, 460 °C, 490 °C, 520 °C and 550 °C as well as for 0 h (heated up to 550 °C and quenched), 4 h, 16 h, 36 h, 72 h and 96 h at 550°C.

As-cast and homogenized samples were mechanically polished according to standard metallographic procedures. The grain microstructure of as-cast sample was characterized using polarized light in a Reichert-Jung optical microscope (OM) following anodization in Barker's reagent. Grain size was determined by linear intercept method according to the standard ASTM E112.

Mechanically polished as-cast sample, samples that underwent selected homogenization treatments: 16 h/490 °C, 4 h/550 °C, 16 h/550 °C, 96 h/550 °C, as well as the sample heated up to 550 °C (0h/550 °C) were examined using a FEG SEM/EDS FEI Scios 2 Dual Beam electron microscope equipped with EDS detector at 15 kV. Microconstituent characterization was performed in chemically sensitive back-scattered electron (BSE) mode, coupled with energy-dispersive spectroscopy (EDS).

Table 1. *Chemical composition of the studied AA5182 alloy / wt.%*

Mg	Mn	Cu	Fe	Si	Zn	Cr	Na	Ti	Zr
4.217	0.46	0.018	0.323	0.137	0.048	0.072	/	0.014	<0.001
±0.056	±0.005	±0.03	±0.014	±0.004	±0.003	±0.005		±0.003	

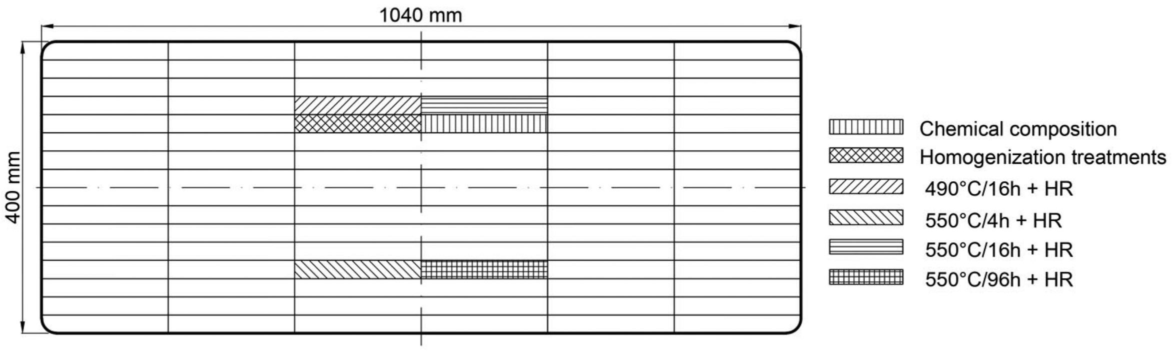

Figure 1. *Schematic presentation the positions of processed blocks within as-cast slice of the studied alloy*

The intensity of the BSE signal, represented as the gray level in micrographs, is proportional to the mean atomic number of the scattering object. Therefore, iron- and manganese-rich particles exhibit lighter contrast than the α-Al matrix, while Mg_2Si particles appear darker. As there are several Fe(Mn)-rich phases differing in the transition-metal content, a variation in gray level among phases is expected. Phases with higher transition-metal content, such as $Al_3(Fe,Mn)$, display higher gray levels or lighter contrast than $Al_6(Fe,Mn)$. Four distinct gray level ranges were identified: 165–180, 197–205, 215–225, and 235–250 for the contrast/brightness conditions used during SEM characterization. These ranges were associated with specific chemical compositions, as determined by semi-quantitative EDS analysis, and unique constituent morphologies, indicating different intermetallic phases. The ratios of Al –vs.– total transition metals content (at%Al/Σat% M_i, where M_i=transition metal) indicated the stoichiometry of intermetallic phases and were in correlation with the expected gray level for each phase justifying the use of gray levels as a criterion for phase identification during image processing. The image processing and stereological measurements were conducted to determine the volume fraction of each type of microconstituent. Adobe Photoshop was used for image processing, including a Median filter (1 pixel radius) to smooth images, followed by multiclass thresholding. In the second step, a high and a low threshold were applied to each type of constituent particles. In the last step, the Median filter (1 pixel radius) was applied again to remove sporadic pixel artifacts. Image J software was employed for image analysis, measuring, among other stereological parameters, the surface area of individual constituent particles and the total area for each phase. Volume fraction, which is equivalent to the area fraction [18], was determined as the ratio of the total area of each constituent class and the total area of the image. The images had the area 500×300 μm^2 and were formed by stitching 4×4 micrographs, providing a broad field of view. 3-5 such images were characterized per state.

The size of the dispersoids is too small compared to the interaction volume of 2 µm at 15 kV [12], so EDS was used only for qualitative analysis to identify the elements present in particles with different morphologies. The number fraction was determined manually by counting the particles. Five fields of view with a size 30×30 μm^2 were characterized for each homogenization regime.

The influence of the four selected homogenization regimes and developed microstructure on restoration processes during subsequent hot-rolling was assessed. Hot-rolling was performed on a lab-scale single-stand mill with a 206 mm roll diameter. It was carried out by ten passes and resulted in a total thickness reduction of 85%. The starting hot-rolling temperature was 490-500 °C. Samples that were homogenized at 550 °C were cooled in the furnace to the rolling temperature. The applied 85% deformation approximates a commercial roughing mill process. It is widely recognized that simulating each stage of industrial hot-rolling in lab conditions has numerous challenges, particularly in maintaining uniform temperature throughout the material during processing. In the roughing mill stage, the ingot typically maintains a nearly constant temperature due to its mass. To offset heat loss, caused by the smaller size of the blocks, samples were held in the furnace for 5 min at 500 °C between consecutive passes.

For microstructural and electron backscattered diffraction (EBSD) characterization, hot-rolled samples were viewed parallel to the longitudinal cross-section defined by the rolling (RD) and normal (ND) directions of the HR plate. In the micrographs and maps presented in the paper, the RD is oriented horizontally, while the ND is oriented vertically.

The grain microstructure of the hot-rolled samples was anodized in Barker's reagent and characterized using polarized light in a Reichert-Jung optical microscope (OM). Samples for electron backscattered diffraction (EBSD) characterization and micro-texture measurements were mechanically polished and subsequently electro-polished in 6% perchloric acid solution (60 ml $HClO_4$, 140 ml H_2O, 800 ml C_2H_5OH) at 20°C and 30 V. The EBSD characterization was conducted in an SEM JEOL JSM-6610LV scanning electron microscope equipped with a Symmetry S3 EBSD detector. The EBSD data were processed using AZtecCrystal 2.2 at the University of Belgrade, Faculty of Mining and Geology. The accelerating voltage was 20 kV, and the scanning step size for the maps was 1.5 µm. Data were collected from regions close to the plate surface and the center. To ensure sufficient data statistics and reliability, EBSD maps were collected by three map scans over different areas of the specimen for each region, with 1500-3000 grains analyzed per map. The rasterized area for each map was 569×426 pixels which is equivalent to 853.5×639 μm^2.

3. Results

3.1. Microstructure of As-cast and Homogenized States

3.1.1. Optical Microscopy of As-cast Microstructure

OM micrographs of the microstructure in the as-cast state are shown in Figure 2. The grain microstructure, as can be seen in Figure 2a, is cellular with a grain size of 140 µm. Coarse, irregularly shaped microconstituents lined inter-cellar boundaries (Figure 2b).

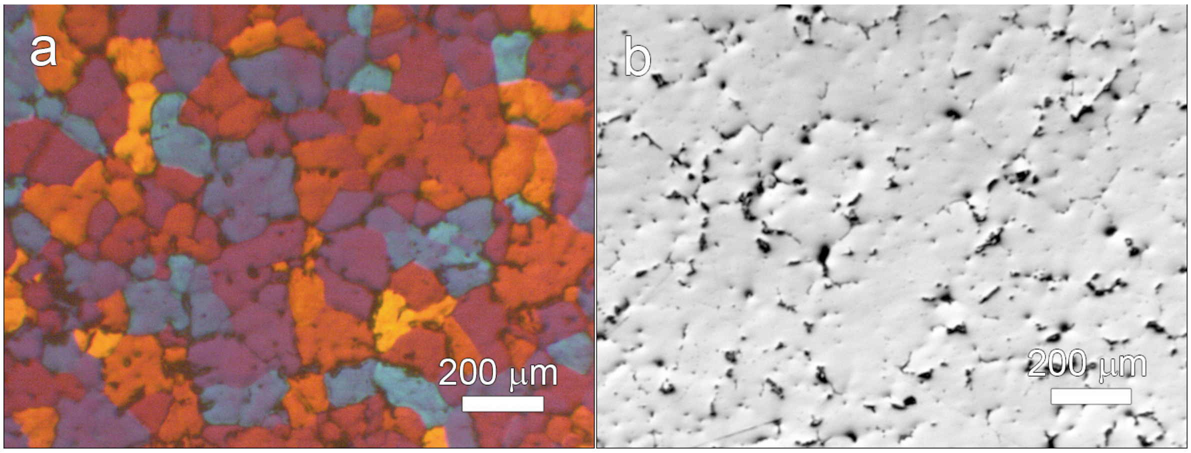

Figure 2. *OM micrographs of the as-cast alloy: (a) grain microstructure in polarized light, and (b) microconstituents in bright field micrographs*

3.1.2. SEM Characterization of Microconstituents

SEM/EDS characterization revealed several constituent phases in the microstructure of the as-cast material. Dark constituents, such as the one shown in Figure 3a, were identified by EDS as Mg_2Si (Figure 3d).

Constituents containing heavier elements, like Fe and Mn, exhibited light contrast with different gray levels in BSE micrographs (Figures 3a-c). The EDS analysis indicated that the gray level is related to a systematic variation in the at%Al/Σat%M_i ratio (M_i represents Fe, Mn, Cr, Ni, Cu, Zn), which is determined by a phase chemical composition (Figures 3d-g and Table 2).

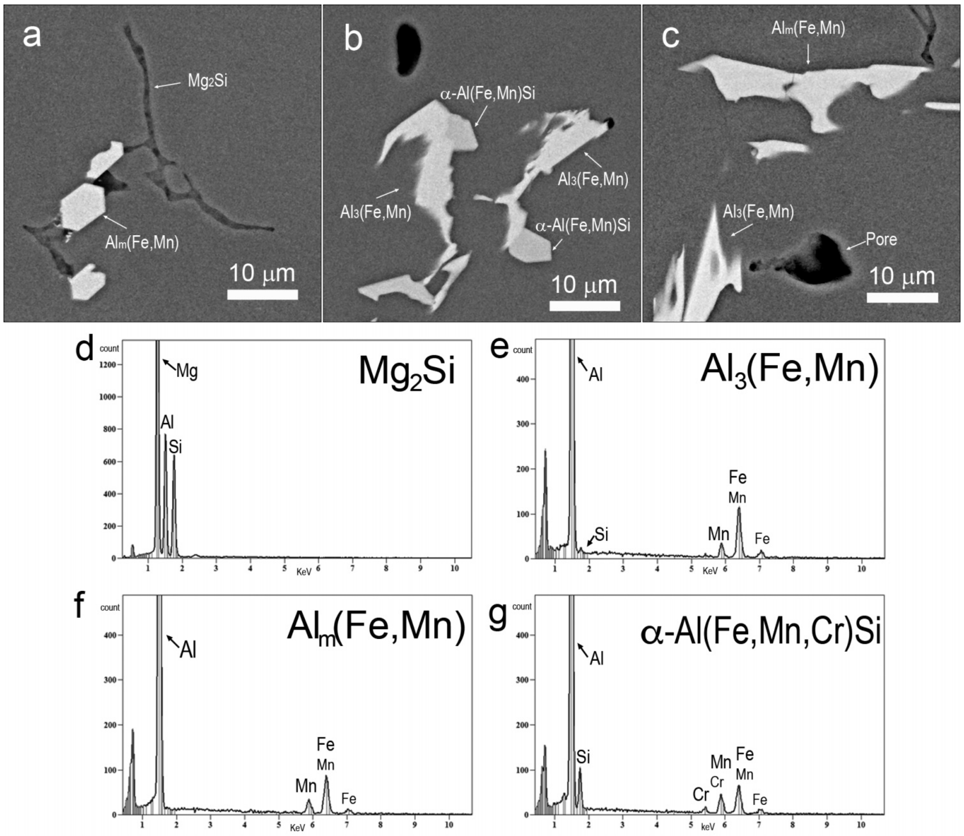

Figure 3. *(a-c) BSE SEM micrographs of microconstituents in as-cast state and (d-g) representative EDS spectra of the selected microconstituents*

Table 2. *Chemistry of Fe/Mn-bearing constituents*

Phase		State					
		As-cast	16 h/490°C	0 h/550°C	4 h/550°C	16 h/550°C	96 h/550°C
$Al_3(Fe,Mn,X)$	at%Al/Σat%Mi*	3.51±0.26	3.56±0.27	3.54±0.13	3.57±0.27	3.60±0.3	3.54±0.14
	at%Fe/at%(Mn+Cr)	3.51±0.43	3.42±0.46	2.9±0.42	3.70±0.94	3.25±0.21	2.77±0.48
	Si, at%	0.34±0.18	0.26±0.10	1.39±0.27	1.48±0.80	0.71±0.29	0.76±0.20
$Al_m(Fe,Mn,X)$ m≈4	at%Al/Σat%Mi*	4.28±0.16	4.86±0.64	5.03±0.11	4.98±0.65	4.59±0.22	/
	at%Fe/at%(Mn+Cr)	2.74±0.25	3.21±0.62	3.78±0.13	4.77±2.98	4.37±3.03	/
	Si, at%	0.00±0.00	0.45±0.62	0.42±0.33	0.72±9.68	0.23±0.23	/
$Al_6(Fe,Mn,X)$	at%Al/Σat%Mi*	/	5.96±0.29	5.76±0.06	5.97	5.75±0.28	5.88±0.29
	at%Fe/at%(Mn+Cr)	/	3.35±1.34	2.64±0.20	2.26	2.02±0.55	1.60±0.41
	Si, at%	/	0.00±0.00	0.00±0.00	0.00±0.00	0.00±0.00	0.00±0.00
α-Al(Fe,Mn,X)Si	at%Al/Σat%Mi*	4.63	5.59±0.93	4.99	4.85±1.25	4.60±0.70	4.64±0.4
	Si, at%	4.78	2.59±0.40	2.35	4.25±1.97	4.46±0.0.57	5.19±0.44
	at% Al/ at% Si	16.28	34.48±3.62	34.1	20.21±3.80	17.48±3.22	15.03±1.23

** Mi represents Fe, Mn, Cr, Ni, Cu, Zn, at%*

The characterization indicated three types of Fe/Mn-bearing constituents in the as-cast material. The constituent, with the lightest contrast (gray level=235-250), characterized by a feathery morphology and sharp, spiky tips (Figures 3b and c), was identified as the $Al_3(Fe,Mn)$ phase. Its at%Al/Σat%M_i ratio ranged from 3.42 to 3.77, which is slightly higher than stoichiometric $Al_{13}Fe_4$. Another light phase (gray level=215-225) with irregular morphology (Figures 3a and c) exhibited at%Al/Σat%M_i ratio in the range of 4-4.4 and was identified as $Al_m(Fe,Mn)$ with m≈4.28 (Table 2). The at%Al/Σat%M_i ratios for both phases were consistent with the compositions reported in [12]. Apart from the difference at%Al/Σat%M_i ratio, more Mn substituted Fe in $Al_3(Fe,Mn)$ than in $Al_m(Fe,Mn)$, and $Al_m(Fe,Mn)$ constituents were virtually free of Si (Table 2). Additionally, small fraction of polygonal faceted phase, rich in Si, was observed (Figure 3b). The approximate composition of these particles, $Al_{16.28}(Fe,Mn)_{3.52}Si$ is indicative of an α-Al(Fe,Mn)Si phase known for varied stoichiometry ranging from $Al_{12}(Fe,Mn)_3Si$ to $Al_{15}(Fe,Mn)_3Si_2$ [8]. Occasionally, a phase with a grayish contrast similar to the matrix was observed, corresponding to β-Al_5Mg_8. This phase, which forms low-melting point with the α-Al matrix, dissolves during heating to homogenization temperatures. No $Al_6(Fe,Mn)$ constituents were detected in the as-cast state.

Homogenization treatments resulted in both compositional and morphological changes of the microconstituents. The principal difference between homogenization at 490 °C and 550 °C is that the lower temperature treatment leads to the additional precipitation of Mg_2Si particles at the interfaces of Fe/Mn-bearing microconstituents (Figure 4a). In contrast, high homogenization temperature causes the coagulation of Mg_2Si microconstituents, which, subsequently, begins to dissolve as homogenization time increased.

$Al_6(Fe,Mn)$ phase, which is absent in the as-cast state, was observed in the material after homogenization at both temperatures (Figure 4). A decrease in the volume fraction of $Al_3(Fe,Mn)$ (Figure 5) and associated morphological changes (Figures 4a-c) indicate an $Al_3(Fe,Mn)$ → $Al_6(Fe,Mn)$ transformation during the homogenization treatment. Figure 4a shows a constituent consisting of interconnected $Al_6(Fe,Mn)$ and $Al_3(Fe,Mn)$ phases. After the homogenization at 550 °C, remains of $Al_3(Fe,Mn)$ phase are seen at the $Al_6(Fe,Mn)$/Al interface grooves (Figure 4b) or as islands surrounded by $Al_6(Fe,Mn)$ (Figure 4c). As the homogenization temperature and time increase, the morphology of the constituents changes from sharp edged to more rounded shapes; longer exposure led to fragmentation. Throughout the transformation, the composition of $Al_3(Fe,Mn)$ changed a little, while $Al_6(Fe,Mn)$ became enriched with Mn as the homogenization temperature and time increased (Table 2).

A fraction of the $Al_m(Fe,Mn)$ constituents also transformed into $Al_6(Fe,Mn)$ phase. However, the remaining $Al_m(Fe,Mn)$ phases underwent more complex changes during homogenization. After homogenization at 490 °C or upon reaching 550 °C, numerous particles exhibiting a lamellar morphology and composition corresponding to $Al_m(Fe,Mn)$ were observed (Figures 6a and d). Unlike the Si-free $Al_m(Fe,Mn)$ found in the as-cast material, these lamellar constituents contained small amounts of Si. Homogenization at 550 °C resulted in new morphology as can be seen in Figures 6b and c.

Figure 6b shows a constituent particle consisting of two distinct regions: a lamellar morphology in the center surrounded by a monolithic region. The EDS of the monolithic regions indicated a higher silicon

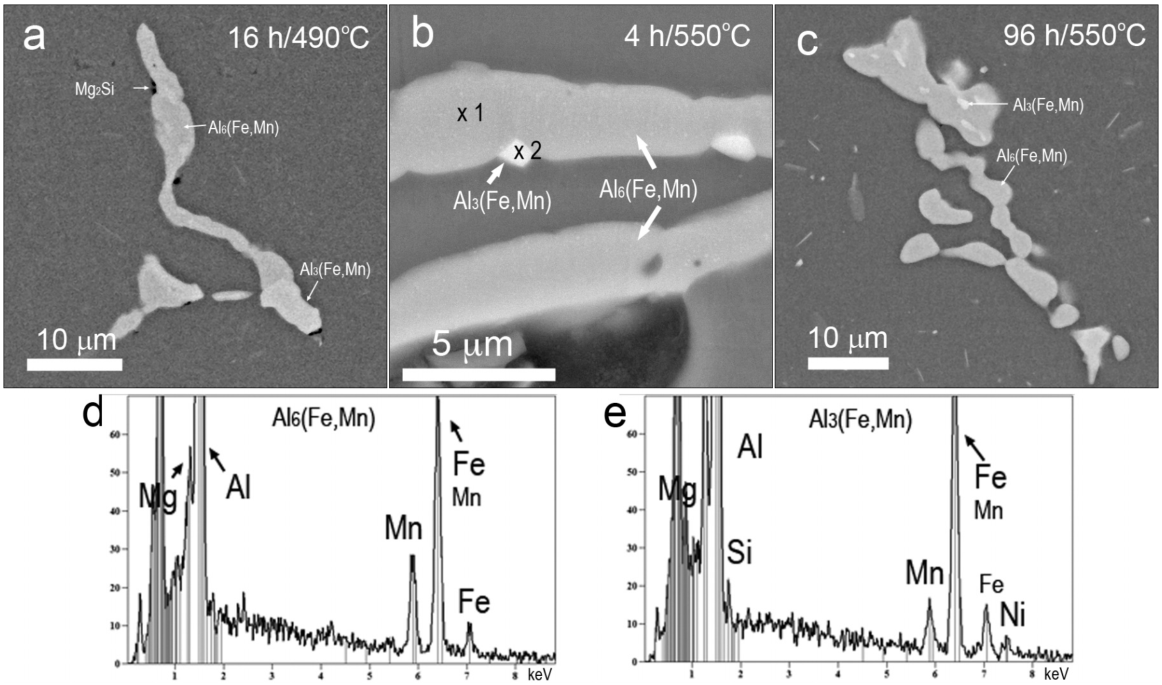

Figure 4. *BSE SEM micrographs of the microconstituents after homogenization: (a) 16 h at 490 °C; (b) 4 h at 550 °C; (c) 96 h at 550 °C. (d-e) EDS spectra of the marked microconstituents shown in (b)*

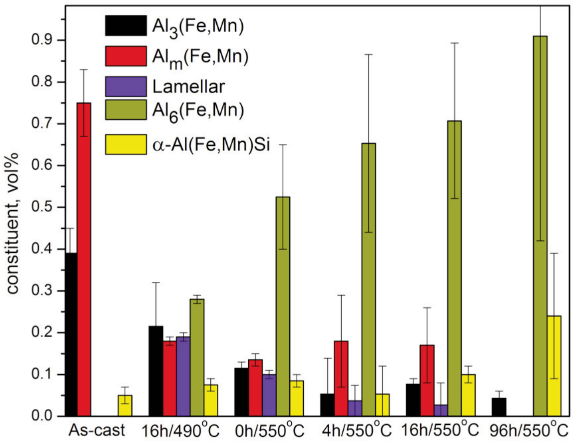

Figure 5. *Plot showing change in volume fraction of constituent particles with homogenization treatment*

content than that observed in the lamellar microconstituent. Prolonging the homogenization treatment led to further shrinking of the lamellar regions and coarsening remaining lamellae (Figure 6c), while the progression of the monolithic regions was accompanied by further Si enrichment (Figures 6e-g). After homogenization of 96 h, the microstructure did not show the presence of particles with lamellar morphology. The newly formed Si-rich phase was classified as α-Al(Fe,Mn)Si although silicon content had not yet reached typical stoichiometry of $Al_{12}(Fe,Mn)_3Si$ to $Al_{15}(Fe,Mn)_3Si_2$ [8]. The plot in Figure 5 summarizes the results of quantitative image analysis. In the as-cast state, the majority of particles had constitution of $Al_m(Fe,Mn)$ phase with a volume fraction 0.75, while the fraction of $Al_3(Fe,Mn)$ was 0.39 vol% (Figure 5). Fraction of α-Al(Fe,Mn)Si phase was very small, 0.05 vol%, as only a few particles were observed. The total fraction of Fe/Mn-bearing microconstituents in the as-cast state was 1.19 vol% and did not significantly change with homogenization. However, variation in the constituent volume fraction in the range 0.5-1.4 vol% in the different regions of the same state indicated the presence of microstructural inhomogeneity in the alloy. As can be seen in Figure 5 fractions of primary constituent phases, $Al_3(Fe,Mn)$ and $Al_m(Fe,Mn)$, continually decreased as homogenization time and temperature increased. $Al_6(Fe,Mn)$ phase particles, while absent in the as-cast alloy, become dominant phase after the homogenization treatments. The fraction of α-Al(Fe,Mn)Si constituents also increased.

3.1.3. Characterization of Dispersoids Evolution during Homogenization

The formation of various Fe,Mn-bearing, and Mg_2Si microconstituent phases depleted the aluminum matrix of solutes during solidification. However, a sufficient level of supersaturation remained, which triggered precipitation reactions during homogenization anneal. The decomposition of the α-Al solid solution and precipitation reactions

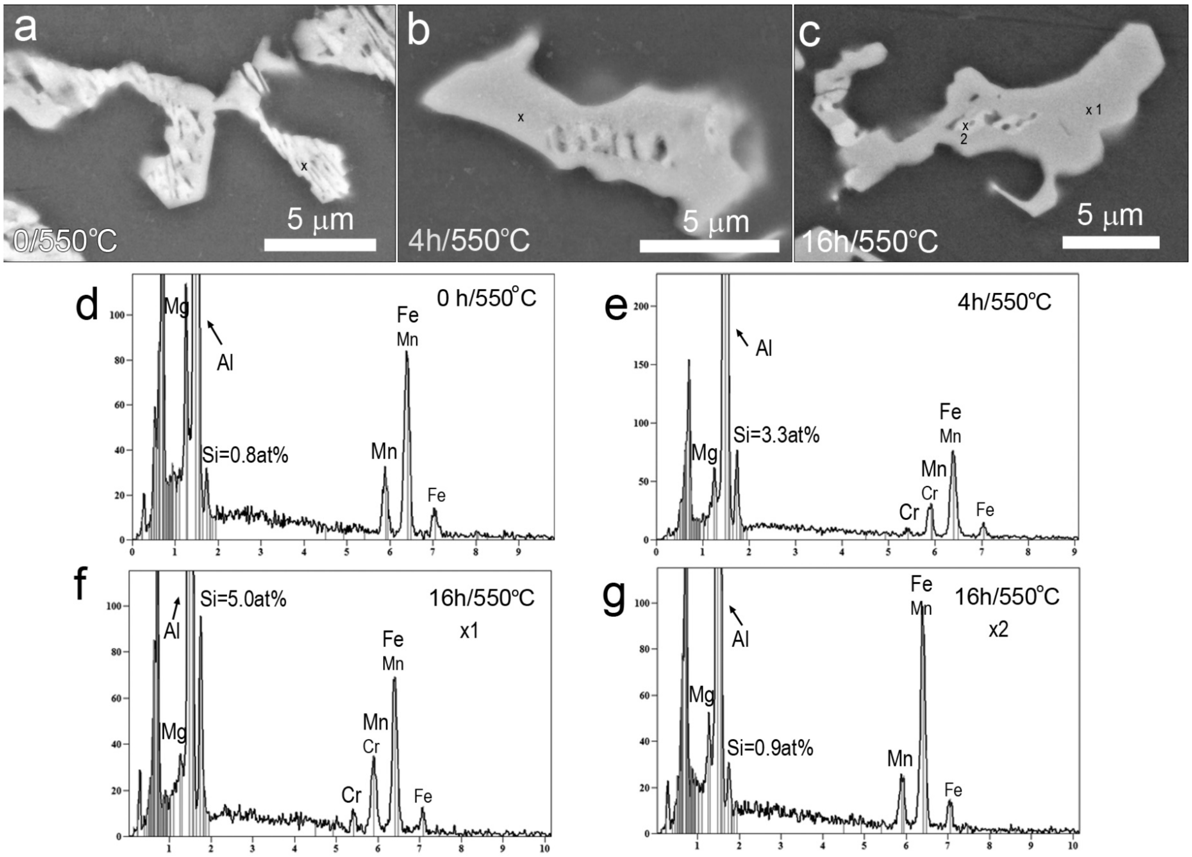

Figure 6. *BSE SEM micrographs illustrating the evolution of the lamellar microconstituents during homogenization: (a) sample was heated up to 550°C; (b) 4 h at 550°C; (c) 16 h at 550°C and (d-g) corresponding EDS spectra*

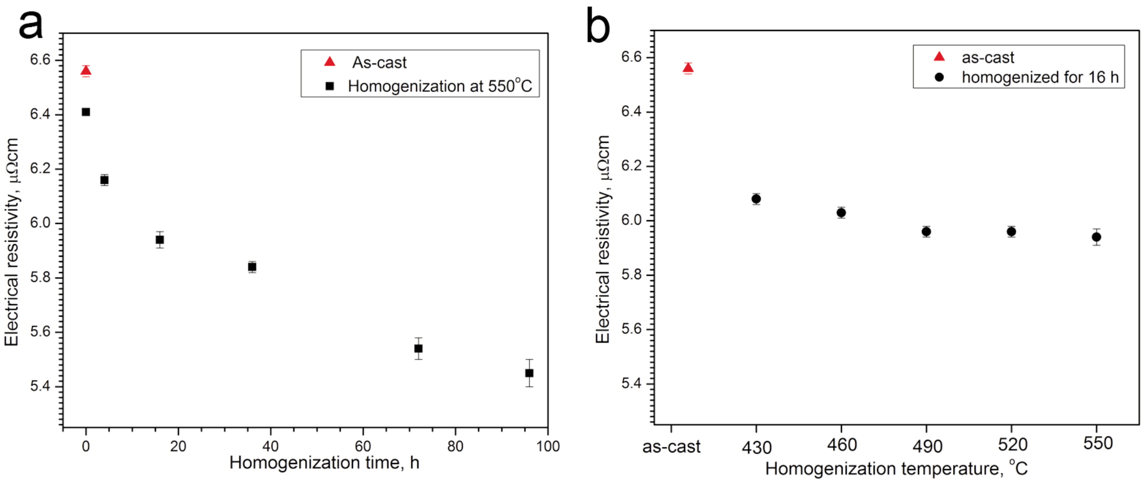

Figure 7. *Plots showing a change in electrical resistance as a function of homogenization conditions: (a) isothermal homogenization at 550 °C, τ=0-96 h; (b) isochronal homogenization (τ=16 h), T=430-550 °C*

were indicated by the electrical resistivity measurements. The electrical resistivity, sensitive to the solute content, is the highest in the as-cast state and showed a continual decrease as homogenization time increased during treatment at 550 °C (Figure 7a). On the other hand, the results of the electrical resistivity measurements on samples annealed for 16 h at different temperatures (Figure 7b) highlighted the complexity of the reactions occurring during the homogenization, which include both precipitation and dissolution processes. There is a continual decrease in the electrical resistivity of the homogenization temperature rises from 430 °C to 490 °C. However, beyond 490 °C, further increases in temperature did not affect electrical resistivity. Impeding stagnation in electrical resistivity at higher temperatures range can be attributed to the behavior of the Mg_2Si phase. As noted in the previous section, treatment at 490 °C resulted in additional precipitation of the phase, while homogenization at 550 °C temperature led to its dissolution increasing the solute level in the aluminum matrix.

Microstructural characterization revealed that the decomposition of the Al solid solution involved the precipitation of fine dispersoids with light contrast (Figure 8a) and coarser particles located at the grain boundaries (Figure 8b). The precipitated dispersoids exhibited two distinct shape types: acicular and more rounded particles (Figure 8a). Although the particles were too small for meaningful quantitative EDS analysis, the EDS spectra indicated a difference in chemistry associated with the particle shape. The typical EDS spectrum of the acicular particles (Figure 8c), in addition to strong Al and Mg peaks originating from the surrounding Al-matrix, exhibited Mn and Fe maxima. Spectra of rounded particles (Figure 8d), showed two additional peaks: a strong Si peak and a weaker Cr peak. Both types of dispersoid particles have been reported in Al-Mg alloys and are classified as $Al_6(Mn,Fe)$ and α-Al(Fe,Mn,Cr)Si [8, 19]. Spectra of grain boundary particles indicated $Al_6(Mn,Fe)$ phase (Figure 8e).

Figures 9(a-b) and 9(c-d) show the distribution of dispersoid particles in the samples that were homogenized for 16 h at 490 °C and 550 °C, respectively. After both treatments, dispersoid-rich zones characterized by a dense population of fine bright dispersoid particles were formed within the interiors of the as-cast cells. In the sample homogenized at 490 °C, the dispersoid population consisted of a mixture of a few micrometers long, thin acicular particles and finer rounded particles. These particles were uniformly distributed within dispersoid-rich zones, showing little variation in size and density between the center and the periphery of the zones (Figures 10a-b). In contrast, after homogenization at 550 °C, the centers of the dispersoid-rich zones contained a denser mixture of fine acicular and rounded particles than their periphery. In addition to being less dense, the particles at the periphery of the zones became coarser and less dense (Figures 10c-d).

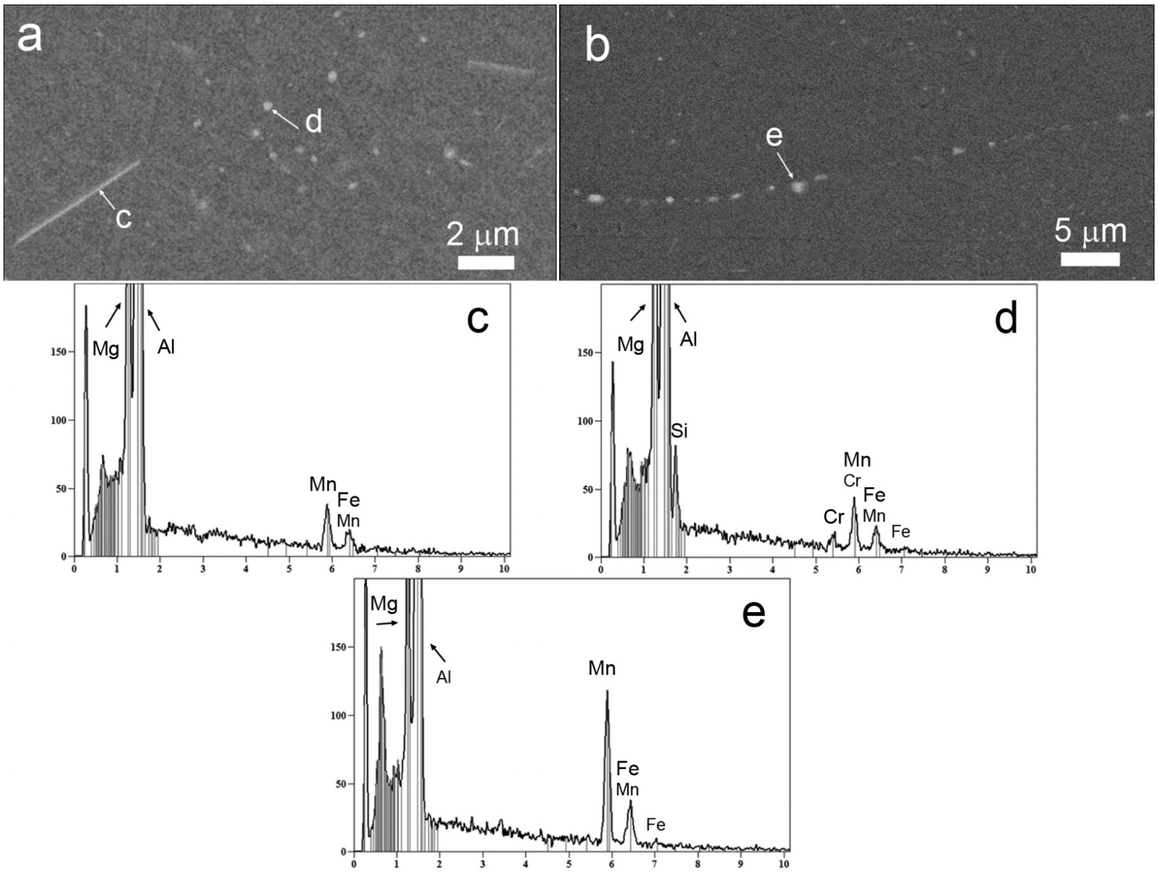

Figure 8. BSE SEM micrographs of precipitated (a) dispersoids in cell interiors, and (b) particles at grain boundaries; (c)-(e) corresponding EDS spectra. Sample was homogenized for 16 h at 550 °C

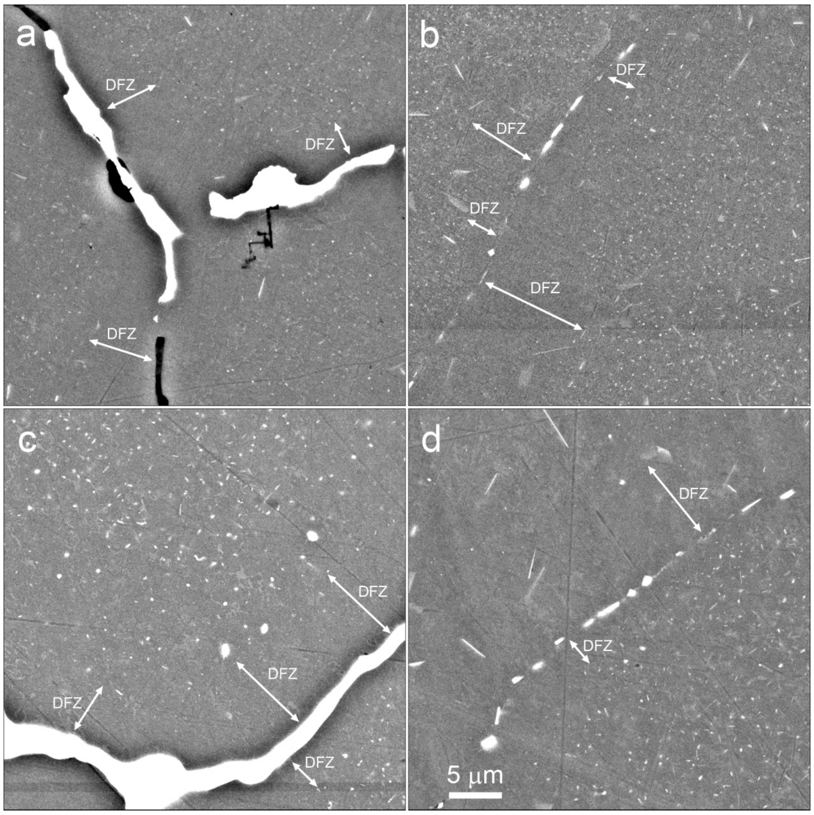

Figure 9. *BSE SEM micrographs showing distribution of dispersoid particles in the samples homogenized for 16 h at (a-b) 490 °C, and (c-d) 550 °C*

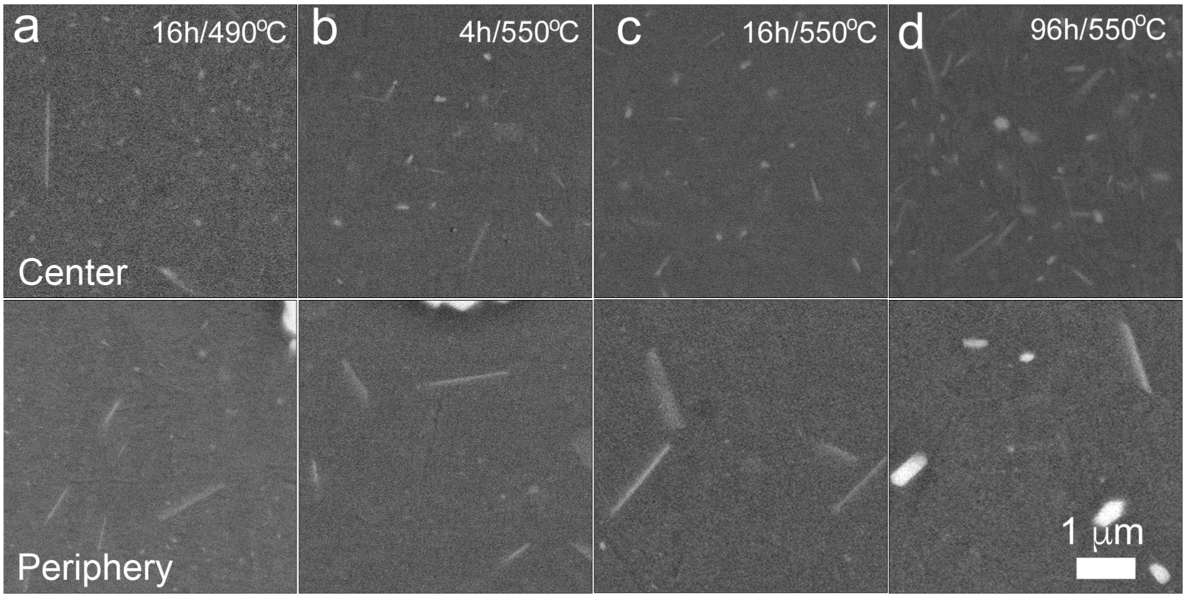

Figure 10. *BSE SEM micrographs of the dispersoids in the center and periphery of dispersoid-rich zones after homogenization: (a) 16 h at 490 °C, and (b) 4 h; (c) 16 h; (d) 96 h at 550 °C*

In the centers of dispersoid-rich zones, the total particle number density remained similar after annealing at 490 °C compared to various treatments at 550 °C, falling in the range of 1-3×10^5 mm^{-3} (Table 3). However, the variation in particle density from one zone to another within the same sample was greater than the variation between samples that underwent different treatments, highlighting the impact of local

Table 3. *Particle density in dispersoid-rich zones and width of dispersoid free zones (DFZ) for different homogenization treatments*

State	16 h/490°C	4 h/550°C	16 h/550°C	96 h/550°C
particle density - acicular, mm^{-3}	1.4×10^4	3.2×10^4	6.6×10^4	12×10^4
particle density -rounded, mm^{-3}	18×10^4	9.2×10^4	15×10^4	20×10^4
particle density, mm^{-3}	19.4×10^4	12.4×10^4	21.6×10^4	32×10^4
DFZ width, μm	7.8	4.6	6.2	8.7

chemistry and microsegregation. The difference in DZ centers between homogenization at 490 °C and treatments at the higher temperature was the increased fraction of fine acicular $Al_6(Mn,Fe)$ particles observed at 550 °C. The longer homogenization time contributed to particle coarsening (Figure 10) and reduction in size of the dense regions within dispersoid-rich zones as well as decrease in particle density at their periphery. For example, approximately 65% of the sample was covered by dispersoid-rich zones after 16 h at 490 °C, whereas this coverage dropped to 40-50% in the sample homogenized 16 h at 550 °C.

3.2. Microstructure and Texture Developed during Hot-rolling

The grain microstructure developed during hot-rolling in samples subjected to different homogenization treatments is shown in Figure 11. Regardless of the homogenization conditions, there is a clear difference in the grain morphology of the region close to the surface and center of the hot-rolled plate, indicating non-uniform deformation. The subsurface region, which experiences a higher strain than the center, appears to undergo a higher degree of recovery and recrystallization. The samples homogenized 16 h at 490 °C and 4 h at 550 °C (Figures 11a and b), are characterized by thin, long grains that have undergone some fragmentation along with occasional small, rounded grains near constituent particles. In contrast, long, deformed grain microstructure in the center of the hot-rolled plate appears almost intact. The restoration processes appear far more advanced in the samples that were annealed for 16 h and 96 h at 550 °C (Figures 11c and d). In these samples, the long grains almost completely disappear, resulting in the microstructure composed of coarser, somewhat elongated grains as well as fine rounded grains in the subsurface region. While some long, deformed grain microstructure remains after homogenization for 16 h at 550 °C in the center of the plate, the microstructure after homogenization for 96 h resembles that of the subsurface region, albeit with coarser grains.

The EBSD characterization of the samples homogenized for 16 h at 490 °C and 550 °C revealed the presence of a deformation texture characterized by strong brass and S components (Figure 12).

The texture was stronger in the sample homogenized at lower temperature. However, the orientation distribution function (ODF) of the subsurface region of the sample treated at 550 °C exhibited additional peaks, specifically a high

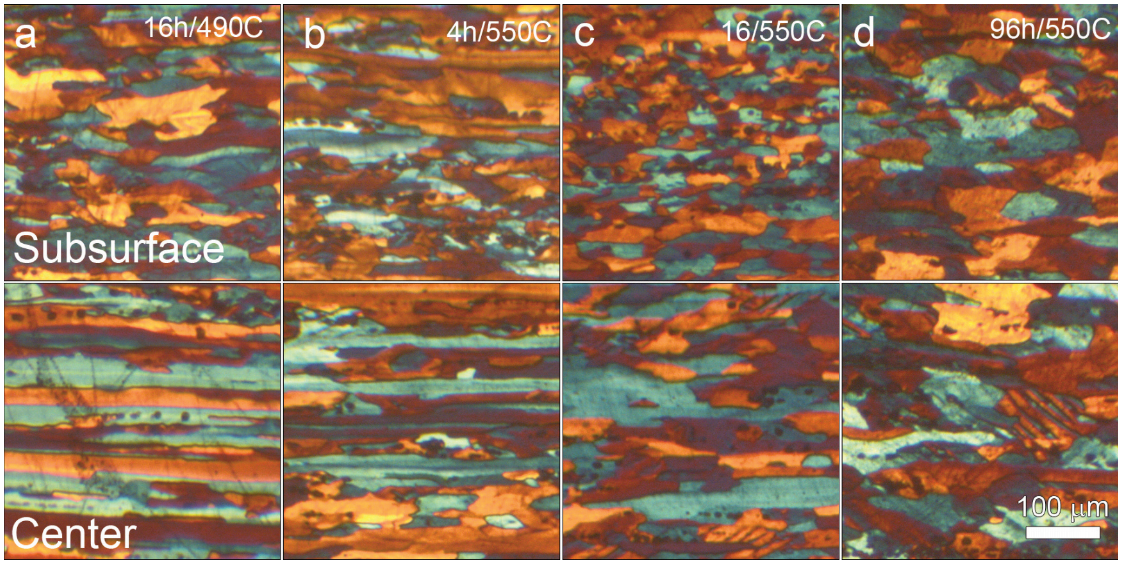

Figure 11. *OM micrographs of the grain microstructure near the surface and in the center of hot-rolled plates homogenized (a) 16 h at 490 °C, and (b) 4 h; (c) 16 h; (d) 96 h at 550 °C*

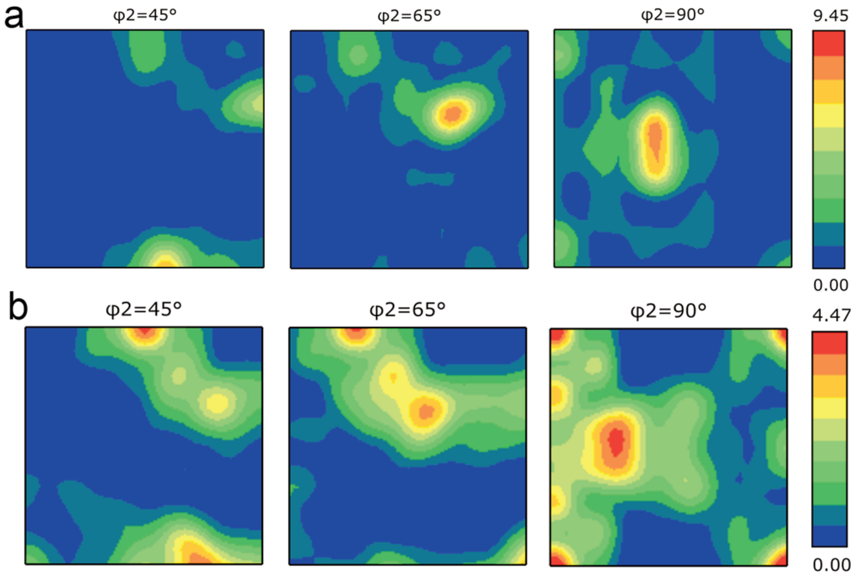

Figure 12. *ODFs of the subsurface region of the hot-rolled plates homogenized (a)16 h at 490 °C, and (b) 16 h at 550 °C*

intensity at cube and cube RD positions indicating the presence of recrystallized grains.

To assess the extent of the recovery and recrystallization, we evaluated Grain Orientation Spread (GOS) maps. GOS represents the average deviation of the orientations of all measured points within a grain relative to the grain's average orientation. In aluminum alloys, GOS values ranging from 1° to 2° are associated with strain-free grains, while grains with GOS values between 2° and 10° have undergone some type of recovery. Those with GOS values greater than 10° indicate deformed microstructure [16, 20–22].

Figures 13a and b show GOS maps of the subsurface regions in the hot-rolled samples that were homogenized for 16 h at 490 °C and 550 °C, respectively. The maps, with maximum GOS values ≈8°, indicate a significant degree of restorative processes in both samples. It can be seen that even the majority of long grains, typical of the deformed state, showed GOS values within the range indicative of recovery.

Optical micrographs suggested the higher fraction of recrystallized grains in the sample homogenized at higher temperature. However, the fraction of the strain-free grains was similar, approximately 12-14%, in both treatments. There was a notable difference in the morphology of these strain-free grains.

In the sample homogenized for 16 h at 490 °C most of the strain-free grains were segments within lamellar grains or individual grains formed at triple or quadruple junctions as shown in Figure 13a. However, a few clusters of small rounded strain free-grains were observed around constituents. The fraction of HAGB bounding the strain-free grains was around 66%. The overall fraction of HAGB in the hot-rolled sample homogenized at 490 °C was about 45%.

In the sample homogenized at a higher temperature, the strain-free grains were mostly small, rounded grains forming clusters around constituent particles, as seen in Figure 13b. The grains within these clusters were predominantly separated by high-angle grain boundaries (HAGB≥15°), with a fraction of HAGB about 89%. In contrast, to the overall fraction HAGB in the microstructure was only 31%.

4. Discussion

According to the CALPHAD simulations, a 2-D section of the Al-Fe-Mn-Si-Mg equilibrium phase diagram, for a similar content of transition metals and Si as in the studied alloy [8], indicates that the stable phase field at the temperatures of interest for high Mg alloys is α-Al+Al_6(Fe,Mn)+Mg_2Si. However, the results of this study revealed that the phases Al_m(Fe,Mn) and Al_3(Fe,Mn) are present in the as-cast state in lieu with the study of Li et al. [23]. Additionally, a small fraction of α-Al(Fe,Mn)Si phase was detected, which is expected to be stable in alloys with lower magnesium content than the nominal composition of the studied alloy according to the phase diagram [8].

The deviation of the constituent phase composition from the equilibrium state is typically attributed to the effect of the solidification rate and microsegregation [8]. Despite this deviation in the as-cast state, several studies have reported either the absence of phase transformation in the constituents [8] or transformation where the metastable Al_m(Fe,Mn) transforms into Al_3(Fe,Mn)+α-Al [23] or

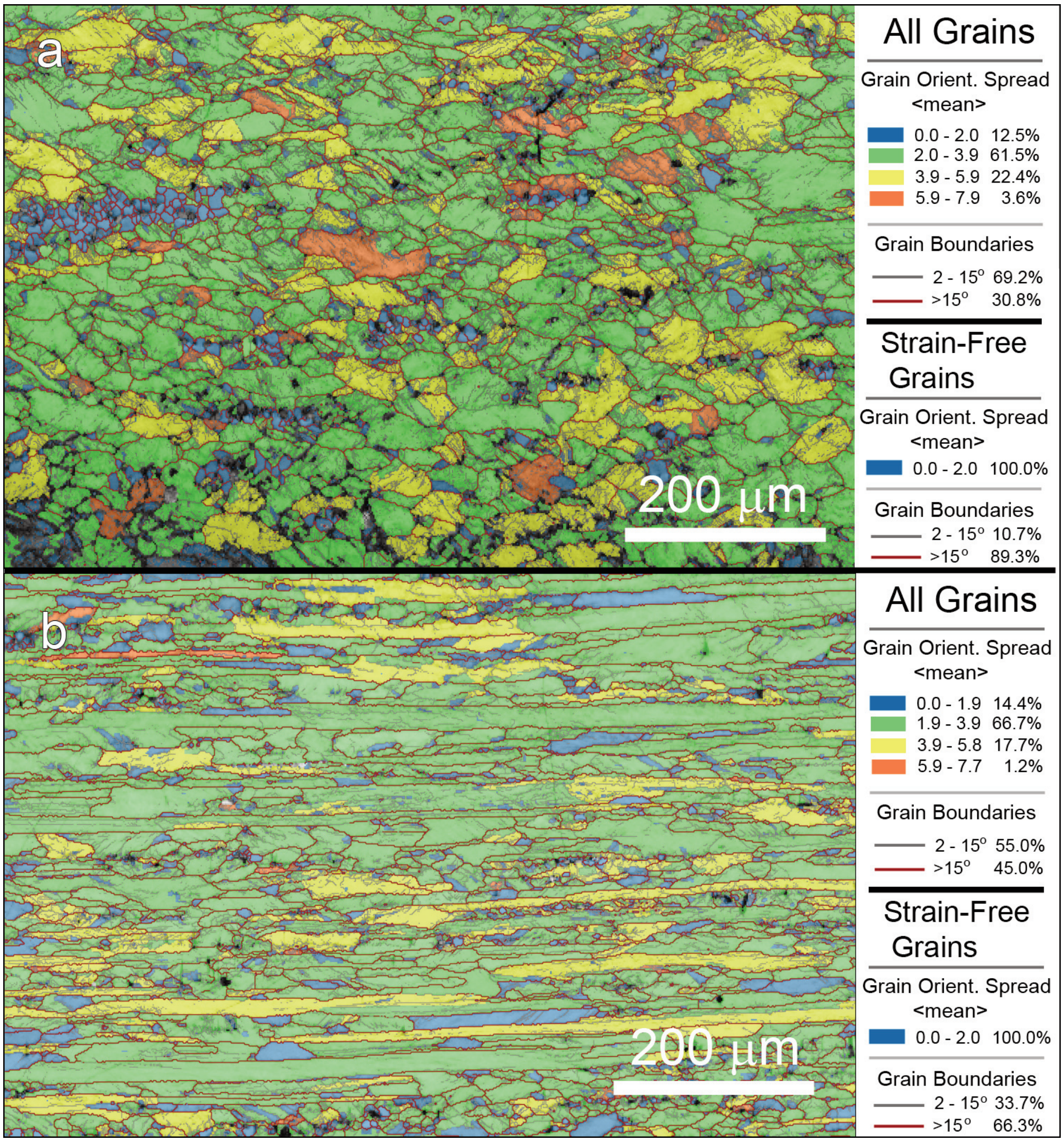

Figure 13. *GOS maps of the subsurface region of the hot-rolled plates homogenized: (a) 16 h at 490 °C, and (b) 16 h at 550 °C*

$Al_{19}(Fe,Mn)_4$' converts into $Al_3(Fe,Mn)$+$Al_{19}(Fe,Mn)_4$ [13]. In contrast to those findings, our results show that primary constituents do transform into $Al_6(Fe,Mn)$ and, to a lesser extent, α-Al(Fe,Mn)Si phase. The difference in behavior is likely influenced by the choice of homogenization treatment parameters, including longer treatment and higher temperatures. The lamellar microconstituent observed at lower homogenization temperature and after shorter homogenization times at 550 °C, is indicative of a eutectoid phase transformation described by Li et al. [23], where $Al_m(Fe,Mn)$ transforms into $Al_3(Fe,Mn)$+α-Al. However, unlike their study, which concludes transformation there, our results indicate that with prolonged homogenization time, the lamellar microconstituent further transforms into a monolithic Si-rich phase. Apparently, the decomposition of the metastable $Al_m(Fe,Mn)$ phase does not stop at eutectoid transformation but continues along this path: $Al_m(Fe,Mn) \rightarrow Al_3(Fe,Mn)+\alpha Al \rightarrow \alpha\text{-}Al(Fe,Mn)Si$.

An increase in homogenization temperature significantly accelerates transformation kinetics. Our results indicate that even after a long homogenization time (16 h) at a low homogenization temperature (490 °C), only a fraction of the primary constituents transformed into Al_6(Fe,Mn) and the composition of the α-Al(Fe,Mn)Si particles deviated from stoichiometric. In contrast, transformation into Al_6(Fe,Mn) begins during heating to 550 °C and it becomes the prevalent phase upon reaching the homogenization temperature (Figure 4).

The transformation into Al_6(Fe,Mn) is not thefinal stage. Once formed, with the extended homogenization treatment, the constituent particles become enriched with manganese, decreasing the Fe/Mn ratio in the compound. As additional manganese originates from the surrounding area, enrichment of constituent particles leads to the formation of dispersoid-free zones (DFZ) and lower particle density at the periphery of the dispersoid-rich zones. The morphology, size, and distribution of dispersoids are known to significantly influence the dynamic recovery and recrystallization of Al-alloys [15, 24]. In the studied alloy, homogenization conditions impacted its microstructure, thereby affecting both the ease of recrystallization and the underlying mechanism. In the samples homogenized for a long time (16-96 h) at 550 °C, the reduction in the size of the particle-dense regions facilitated recovery and recrystallization during early stages of hot-rolling. As a result, the original long deformed grains are sparse, particularly in the subsurface region. However, the recrystallization that occurred during initial rolling passes decreased the stored energy of deformation, which in turn reduced the driving force for recrystallization during the final pass. The final grain microstructure consisted of grains that underwent varied degrees of recovery, while recrystallized regions were primarily located around the constituent particles. Apparently, the dissolution of the dispersoids in vicinity of constituent particles and lower particle density at the periphery of the dispersoid-rich zones favored the particle stimulated nucleation (PSN) mechanism [25] as the primary recrystallization mechanism. In contrast, in the samples homogenized at 490 °C or for a short time (4 h) at 550 °C, PSN mechanism was not efficient due to the uniform distribution of the dispersoid particles. In those samples, recrystallization was inhibited during the early passes, leading to the accumulation of stored energy of deformation that activated other restoration mechanisms. Observation of strain-free grains formed within deformed original grains suggest as subgrain growth [25] as a favored mechanism in these samples.

5. Conclusions

In the present study, various homogenization treatments were conducted to investigate their impact on the recrystallization behavior during laboratory hot-rolling of AA5182 alloy. The following conclusions can be drawn.

- The as-cast microstructure of AA5182 alloy consisted of aluminum cells surrounded by Al_3(Fe,Mn) and Al_m(Fe,Mn) as Fe/Mn-bearing microconstituents along with Mg_2Si.
- During the homogenization treatments at both 490 °C and 550 °C, the primary constituent phases transformed into Al_6(Fe,Mn) and α-Al(Fe,Mn)Si. The extent of this transformation was dependent on the treatment time and temperature.
- The eutectoid transformation of Al_m(Fe,Mn) resulted in lamellar Al_3(Fe,Mn)+Al, which subsequently transformed into α-Al(Fe,Mn)Si phase.
- At 550 °C, longer treatment times led to an enrichment of the newly formed Al_6(Fe,Mn) phase with manganese. This was followed by an increase in the width of the DFZ and a decrease in the dispersoid particle density at the periphery of dispersoid-rich zones.
- The recrystallization mechanism during hot-rolling appears to be sensitive to the dispersoid particle density. The PSN mechanism appears to be favored when there is decrease in size of dispersoid-rich zones and in the presence of lower particle density at their periphery, while subgrain growth occurs in the presence of uniformly dense dispersoid-rich zones.

Acknowledgement

This work was supported by the Ministry of Science, Technological Development and Innovation of the Republic of Serbia under contract No. 451-03-136/2025-03/200135.

D.P. acknowledges the Science Fund of Serbia for funding this research through project RECON TETHYS (7744807).

Author Contributions

A. Ćitić: Investigation, Writing-original draft; T. Radetić: Conceptualization, Methodology, Writing-Review & Editing, Filip Rajković: Investigation, Dejan Prelević: Validation; M. Popović: Editing, Supervision.

Data Availability

The data are available from the corresponding author upon reasonable request.

Conflicts of Interest

The authors declare no conflict of interest.

References

[1] O. Engler, S. Miller-Jupp, Control of second-phase particles in the Al-Mg-Mn alloy AA 5083, Journal of Alloys and Compounds, 689 (2016) 998-1010. https://doi.org/10.1016/j.jallcom.2016.08.070

[2] E. Romhanji, T. Radetić, M. Popović, Homogenization of an Al-Mg alloy and alligatoring failure: alloy ductility and fracture, Materiali in Tehnologije, 50 (3) (2016) 403-407. https://doi:10.17222/mit.2015.110

[3] E. Romhanji, T. Radetić, M. Popović, Homogenization of an Al-Mg alloy and alligatoring failure: influence of the microstructure, Materiali in Tehnologije, 50 (4) (2016) 531-536. https://doi:10.17222/mit.2015.111

[4] A.Y. Algendy, K. Liu, X. Grant Chen, Evolution of dispersoids during multistep heat treatments and their effect on rolling performance in an Al-5% Mg-0.8% Mn alloy, Materials Characterization, 181 (2021) 111487. https://doi.org/10.1016/j.matchar.2021.111487

[5] L. Tan, T.R. Allen, Effect of thermomechanical treatment on the corrosion of AA5083, Corrosion Science, 52 (2) (2010) 548-554. https://doi.org/10.1016/j.corsci.2009.10.013

[6] R. Goswami, G. Spanos, P.S. Pao, R.L. Holtz, Precipitation behavior of the ß phase in Al-5083, Materials Science and Engineering A, 527 (4-5) (2010) 1089-1095. https://doi.org/10.1016/j.msea.2009.10.007

[7] A. Verma, S. Kumar, P.S. Grant, K.A.Q. O'Reilly, Influence of cooling rate on the Fe intermetallic formation in an AA6063 Al alloy, Journal of Alloys and Compounds, 555 (2013) 274-282. https://doi.org/10.1016/j.jallcom.2012.12.077

[8] O. Engler, K. Kuhnke, J. Hasenclever, Development of intermetallic particles during solidification and homogenization of two AA 5xxx series Al-Mg alloys with different Mg contents, Journal of Alloys and Compounds, 728 (2017) 669-681. https://doi.org/10.1016/j.jallcom.2017.09.060

[9] O. Engler, K. Kuhnke, K. Westphal, J. Hasenclever, Impact of chromium on the microchemistry evolution during solidification and homogenization of the Al-Mg alloy AA 5052, Journal of Alloys and Compounds, 744 (2018) 561-573. https://doi.org/10.1016/j.jallcom.2018.02.125

[10] A.Y. Algendy, K. Liu, X.-Grant Che, Formation of intermetallic phases during solidification in Al-Mg-Mn 5xxx alloys with various Mg levels, MATEC Web of Conferences 326 (2020) 02002. https://doi.org/10.1051/matecconf/202032602002

[11] C.J. Simensen, U. Södervall, Investigation of trace elements in an Al–4.8 wt.% Mg–0.3 wt.% Mn alloy, Surface and Interface Analysis, 30 (1) (2000) 309-314. https://doi.org/10.1002/1096-9918(200008)30:1<309::AID-SIA806>3.0.CO;2-Y

[12] Y.J. Li, L. Arnberg, Solidification structures and phase selection of iron-bearing eutectic particles in a DC-cast AA5182 alloy, Acta Materialia, 52 (9) (2004) 2673-2681. https://doi.org/10.1016/j.actamat.2004.02.015

[13] N. Tian, Y. Zhang, Z.He, H. Liu, Z. Zhang, J. Liu, G. Zhaoa, G. Qin, The formation of three phases containing Fe and Mn in 5182 aluminum alloy, Materials Characterization, 207 (2024) 113497. https://doi.org/10.1016/j.matchar.2023.113497

[14] V. Aryshenskii, F. Grechnikov, E. Aryshenskii, Y. Erisov, S. Konovalov, M. Tepterev, A. Kuzin, Alloying elements effect on the recrystallization process in magnesium-rich aluminum alloy, Materials, 15 (20) (2020) 7062. https://doi.org/10.3390/ma15207062

[15] A.Y. Algendy, K. Liu, X.-Grant Chen, Effect of Mn-bearing dispersoids on tensile properties and recrystallization resistance of Al-3Mg-0.8Mn rolled alloy, Advanced Engineering Materials, 25 (19) (2023) 2300667. https://doi.org/10.1002/adem.202300667

[16] Y.J. Li, W.Z. Zhang, K. Marthinsen, Precipitation crystallography of plate-shaped Al_6(Mn,Fe) dispersoids in AA5182 alloy, Acta Materialia, 60 (17) (2012) 5963-5974. https://doi.org/10.1016/j.actamat.2012.06.022

[17] B. Raeisinia, W.J. Poole, D.J. Lloyd, Examination of precipitation in the aluminum alloy AA6111 using electrical resistivity measurements, Materials Science and Engineering A, 420 (1−2) (2006) 245–249. https://doi.org/10.1016/j.msea.2006.01.042

[18] E.E. Underwood, Quantitative stereology in microstructural analysis (J.L. McCall, W.M. Mueller), Springer, Boston, 1973, p. 35-66. https://doi.org/10.1007/978-1-4615-8693-7_3

[19] K. Li, T. Zou, D. Li, Y. Peng, D. Shu, On formation of abnormally large grains in annealing prestrained aluminum alloy multiport extrusion tubes, Metallurgical and Materials Transactions A, 50 (12) (2019) 5734-5749. https://doi.org/10.1007/s11661-019-05453-0

[20] H. Zhao, L. Sun, G. Zhaoa, J. Yu, F. Liu, X. Sun, Z. Lv, S. Cao, Abnormal grain growth behavior and mechanism of 6005A aluminum alloy extrusion profile, Journal of Materials Science and Technology, 157 (2023) 42-59. https://doi.org/10.1016/j.jmst.2023.02.013

[21] L. Chen, S. Zhang, Z. Li, G. Zhao, C. Zhang, J. Lin, Investigation on peripheral coarse grains and precipitation behavior of in-situ TiB_2/Al–Cu–Mg composites with various Mg contents, Materials Science and Engineering A, 826 (2021) 142000. https://doi.org/10.1016/j.msea.2021.142000

[22] Y. Wang, B. Yang, M. Gao, R. Guan, Deformation behavior and dynamic recrystallization during hot compression in homogenized Al–6Mg–0.8Mn alloys, Materials Science and Engineering A, 840 (2020) 142953. https://doi.org/10.1016/j.msea.2022.142953

[23] Y.J. Li, L. Arnberg, A eutectoid phase transformation for the primary intermetallic particle from Al_m(Fe,Mn) to Al_3(Fe,Mn) in AA5182 alloy, Acta Materialia, 52 (10) (2004) 2945-2952. https://doi.org/10.1016/j.actamat.2004.02.041

[24] E.V. Aryshenskii, J. Hirsch, S.V. Konvoalov, U. Prahl, Specific features of microstructural evolution during hot rolling of the as-cast magnesium-rich aluminum alloys with added transition metal elements, Metallurgical and Materials Transactions A, 50(12) (2019) 5782-5799. https://doi.org/10.1007/s11661-019-05480-x

[25] J. Humphreys, J.S. Rohrer, A. Rollett, Recrystallization and related phenomena, Elsevier Ltd., 2017, p.321-508.

EVOLUCIJA MIKROSTRUKTURE POD RAZLIČITIM USLOVIMA HOMOGENIZACIJE I NJEN UTICAJ NA PROCESE REKRISTALIZACIJE TOKOM TOPLOG VALJANJA LEGURE AA5182

Aleksandar Ćitić [a,b], Tamara Radetić [a], Filip Rajković [c], Dejan Prelević [c], Miljana Popović [a,*]

[a] Univerzitet u Beogradu, Tehnološko-metalurški fakultet, Beograd, Srbija
[b] Vojnotehnički institut, Beograd, Srbija
[c] Univerzitet u Beogradu, Rudarsko-geološki fakultet, Beograd, Srbija

Apstrakt

Ova studija ispituje razvoj mikrostrukture legure AA5182 Al–Mg pri različitim uslovima homogenizacije kao i uticaj tih uslova na procese rekristalizacije i razvoj teksture tokom laboratorijskog toplog valjanja. Homogenizacija je sprovedena u trajanju od 16 h na 490 °C, kao i u trajanju od 4 h, 16 h i 96 h na 550 °C. Karakterizacija primenom skenirajuće elektronske mikroskopije (SEM), uključujući energijski disperzivnu rendgensku spektroskopiju (EDX), otkrila je prisustvo faza $Al_3(Fe,Mn)$ *i* $Al_m(Fe,Mn)$ *kao mikro-konstituenata koji sadrže Fe/Mn u livenom stanju. Tokom homogenizacije ove faze su transformisane u* $Al_6(Fe,Mn)$ *i* α*-Al(Fe,Mn)Si. Različiti tretmani doveli su do izdvajanja disperzoidnih čestica* $Al_6(Mn,Fe)$ *i* α*-Al(Fe,Mn)Si. Rezultati difrakcije povratno rasejanih elektrona (EBSD) ukazali su na prisustvo slabe deformacione teksture nakon toplog valjanja. Morfologija zrna i stepen restauracije bili su značajno uslovljeni parametrima homogenizacije. Raspodela i gustina disperzoida snažno su uticale na mehanizme oporavljanja i rekristalizacije.*

Ključne reči: *Legura AA5182; Homogenizacija; Mikro-konstituenti sa (Fe,Mn); Disperzoidi sa Mn; Rekristalizacija*